HAL
open science

Modeling the spatio-temporal evolution of permeability during coking of porous material

Eddy El Tabach, Khaled Chetehouna, Nicolas Gascoin, Florian Gaschet, Guillaume Fau

To cite this version:

Eddy El Tabach, Khaled Chetehouna, Nicolas Gascoin, Florian Gaschet, Guillaume Fau. Modeling the spatio-temporal evolution of permeability during coking of porous material. 20th AIAA International Space Planes and Hypersonic Systems and Technologies Conference (Hypersonics 2015), 6-9 July 2015, Glasgow, Scotland, AIAA-2015-3664, 2015, glasgow, France. 10.2514/6.2015-3663 . hal-01253379

HAL Id: hal-01253379

https://hal.science/hal-01253379v1

Submitted on 19 Feb 2016

HAL is a multi-disciplinary open access archive for the deposit and dissemination of scientific research documents, whether they are published or not. The documents may come from teaching and research institutions in France or abroad, or from public or private research centers.

L'archive ouverte pluridisciplinaire **HAL**, est destinée au dépôt et à la diffusion de documents scientifiques de niveau recherche, publiés ou non, émanant des établissements d'enseignement et de recherche français ou étrangers, des laboratoires publics ou privés.

Modeling the spatio-temporal evolution of permeability during coking of porous material

Eddy EL TABACH[1]
Univ. Orléans, IUT-Bourges, PRISME EA 4229, F-18000 Bourges, France

Khaled CHETEHOUNA[2]
INSA-CVL, Univ. Orléans, PRISME EA 4229, F-18022 Bourges, France

Nicolas GASCOIN[3]
INSA-CVL, Univ. Orléans, PRISME EA 4229, F-18022 Bourges, France

Florian GASCHET[4]
Univ. Orléans, IUT-Bourges, PRISME EA 4229, F-18000 Bourges, France

and

Guillaume FAU[5]
INSA-CVL, Univ. Orléans, PRISME EA 4229, F-18022 Bourges, France

Transpiration cooling is one of the most efficient cooling techniques, but one which generates complex phenomena that are difficult to model, and this all the more in that a reactive fluid such as an endothermic fuel is used. Above a certain temperature, such fuel is pyrolysed and, thanks to its endothermic behaviour, this ensures the active cooling of the hot walls of the combustion chamber. However, one of the consequences of this thermal decomposition is the unwanted formation of coke which blocks the porous material (both on the surface and in the interior). This gradual blocking reduces the material's permeability and thus the efficiency of the cooling system. Modelling the permeability distribution of porous materials is thus a key parameter in better understanding transpiration cooling. The present article shows several models intended to estimate the variation in time and space of the permeability of a material (stainless steel) during its coking. The fluid circulating in this porous material is n-dodecane that is maintained at a high temperature. Following a presentation of the measurement device and the measured experimental data of the mean permeability, two categories of model are studied, notably discontinuous mesh models (with 2 and 3 meshes) and continuous analytical models (linear and exponential). The results obtained show that discontinuous models with 2 and 3 meshes are very close in measuring the temporal evolution of the thickness of the coked zone of the porous material. They also revealed that the exponential model is more appropriate than the linear model in estimating the spatiotemporal evolution of the permeability. Additionally, the evolution of the coking rate in the porous material was determined as a function of time and the results show behaviour similar to that indicated in the literature. Lastly, the average Darcy permeability was linked to the mass of coke deposit in the porous material, the result of which reveals a quasi-linear decrease.

[1] Associate Professor, DMS Group, PRISME Laboratory, eddy.el-tabach@univ-orleans.fr.
[2] Tenure Professor, CE Group PRISME Laboratory, khaled.chetehouna@insa-cvl.fr.
[3] Full Professor, CE Group, PRISME Laboratory, nicolas.gascoin@insa-cvl.fr, Senior AIAA Member.
[4] Master student, CE Group, PRISME Laboratory, florian.gaschet@insa-cvl.fr.
[5] Research engineer, CE Group, PRISME Laboratory, guillaume.fau@insa-cvl.fr.

Nomenclature

Latin letters

e	=	Sample thickness
e_j *[m]*	=	Thickness of each layer *j*
K	=	Hydraulic conductivity tensor
K_D	=	Darcian's permeability
K_{Davg}	=	Average Darcian permeability
K_{D0}	=	Initial Darcian permeability
K_F	=	Forchheimer's permeability
K_j	=	Darcian permeability of each layer *j*
P	=	Pressure
ΔP	=	Pressure drop
t	=	time
T	=	temperature
V	=	Mean fluid velocity

Greek Letters

ε	=	Overall open porosity
μ	=	Dynamic viscosity
ρ	=	Fluid density
ø	=	Diameter

I. Introduction

In aerobic vehicules for hypersonic flights (i.e. a flight speeds exceeding Mach 5), the combustion chamber of the continuous flow engine is subjected to extreme heat stress. This results in difficulties in ensuring the mechanical strength of the combustion chamber. To overcome this problem, one technique found in the literature consists in injecting a fluid onto the porous walls of this combustion chamber so as to cool them. When the cooling fluid is nonreactive, the material's permeability and porosity have constant values. However, this is not be the case when the cooling fluid is an endothermic fuel used to supply the combustion chamber. Transporting a single fluid to ensure supply as well as cooling of the combustion chamber enables aerobic vehicles for hypersonic flight to be made lighter. The fuel circulating around the porous walls of the combustion chamber is subjected to high temperature gradients leading to its thermal decomposition[1]. This pyrolysis results in the formation of coke (particles of carbon) on the surface of the porous material which subsequently gradually blocks up the material over time and space. This leads to a certain spatiotemporal distribution of the porosity and permeability in this porous structure which gradually becomes heterogeneous. Modelling the evolution of the permeability of porous materials is thus of great interest in better understanding the decrease in efficiency of the active transpiration cooling system[2,3].

Different studies can be found in the literature related to the determination of the variability of local permeabilities (or of the transmissivity, if two-dimensional flow problems are to be studied) of porous media[4]. The great majority of the studies were performed in the hydrogeological field to describe the heterogeneity of the soil[5,6]. Various methods can be found the simplest of which use algebraic means: arithmetic, geometric and harmonic.

The latter enable a mean permeability to be determined from local permeabilities. Using a deterministic approach, where the field of permeability $K_D(x)$ is sufficiently simple (as is the case, for example, of stratified media that are composed of even layers of permeability juxtapositioned in space) and whose boundary conditions are assumed to be known, exact analytical solutions do exist. In the more general case, the diffusivity equation $\mathrm{div}(K.\mathrm{grad}(h))=0$ is solved numerically. The analytical resolution of this equation is, indeed, possible in the case of uniform flows in stratified media. The two most known results are the equivalent permeability of a flow that is perpendicular or parallel to the strata. If the layers (or strata) are in parallel with respect to the flow direction then the mean permeability is the arithmetic mean of the local permeabilities. If the layers are in series with respect to the flow direction, then the mean permeability is the harmonic mean of the local permeabilities[7]. When the flow is uniform and is both perpendicular and parallel to the strata, the mean permeability is the geometric mean of the local permeabilities[8].

In addition to those in the hydrogeological field, there are studies in the literature relating to the spatio-temporal variation of the permeability in porous materials[9,10]. Uh and Watson (2011) determined the spatial evolution of the

permeability in a bone sample by using Magnetic Resonance Imagery (MRI) and by solving an inverse problem. Martin III et al. (2014) studied the impact of a vertical porosity distribution on the overall permeability of a pervious concrete. They determined by experimentation the evolution of the permeability as a function of the depth of the material by using an image analysis technique described in an earlier work[11].

In previous works[2,12], we experimentally determined the mean permeability by using the Brinkman equation. Several porous materials through which both reactive and nonreactive fluids flow were examined, as was the effect of temperature. The results of this work show that in the case of a reactive fluid, a layer of coke is formed on the material thereby leading to a temporal variation in the mean permeability. Based on these findings, the aim of this article is to study the spatial and temporal distribution of the local permeability of a material as it is being coked (becoming blocked by a layer of coke). The present article is organised as follows. The first section is devoted to the presentation of the experimental data of the mean permeability. The experimental device, the type of material, the reactive fluid, and also the operational conditions are described. This section also explains the theoretical approaches that enable the local permeability to be determined as a function of space and time. The second section reviews the findings and outlines the interpretations. The article will conclude with the prospects for future studies.

II. Equipment and methods

A. Presentation of experimental data of mean permeability

The purpose of the test bench is to study within a laboratory the phenomena that can be expected on the engine by imitating the flight conditions as closely as possible (Fig. 1). Hydrocarbon pyrolysis is possible in pressure conditions of between 10 to 60 bars, from room temperature to 900°C, and at fluid flow rates of $0.05 g.s^{-1}$ to $0.5 g.s^{-1}$. Certain conditions can be met so as to study hydrocarbon pyrolysis in its supercritical phase. The device enables the constant monitoring of these flow rates, pressures and temperatures[1]. It is important to note that the test bench is adapted to thin samples (less than 3 mm) to avoid the uncontrolled lateral permeation on thicker heterogeneous samples[13]. During the trials, the combustible liquid is injected by a pump (80 bars, $0.5 g.s^{-1}$) inside a chemical reactor positioned in a furnace. This reactor is formed of a preheated stainless steel tubular reactor (inside diameter = 3.45mm, length = 550mm) and a cell (inside ∅ =30 mm, length=100mm), into which the porous medium is inserted (filtration diameter only 16 mm). Upon exiting the cell, the tube is cooled and transports the fluid to a phase separator. The liquid phase and the gaseous phase are thus analysed separately and transitionally.

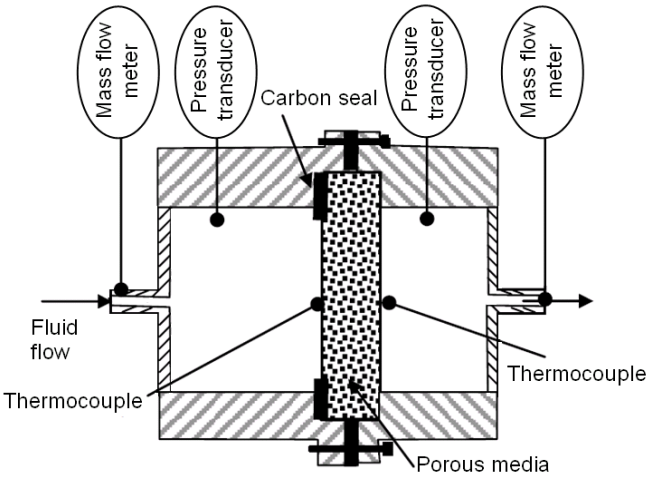

Figure 1. The permeation test cell.

The fluid used in the experiments was n-dodecane (VWR, Rectapur 99% of purity) as this is known to be very representative of kerosene. It has been extensively studied by the authors in numerous pyrolysis configurations[2]. The porous support used was a sample of stainless steel (∅ = 30 mm, filtration diameter = 16 mm thickness of 3 mm) supplied by Federal Mogul (Poral class). This was chosen because it has a more homogeneous morphological structure and is thus easier to study than composite materials. It has an overall porosity of 30%, a pore diameter is of 4.1µm and a grain size of 14.1µm[1]. The test conditions were as follows. For a given mass flow ($65 mg.s^{-1}$), the furnace temperature is raised from room temperature to 750K, then by increments of 50K, after thermal stabilisation

(approximately 45 minutes for each plateau). The pressure within the process was set at 35 bars using a pressure regulator. Three furnace temperature settings were studied (750K, 800K and 850K), which correspond respectively to maximal fluid temperatures of 725K, 765K and 820K.

Knowing the flow rates and pressure drops at all instants and based on the Brinkman equation[14], we were able to estimate the evolution of the average Darcy permeability versus time. Figure 2 shows the evolution versus time of the average Darcy permeability K_{Davg} and the temperature of the n-dodecane.

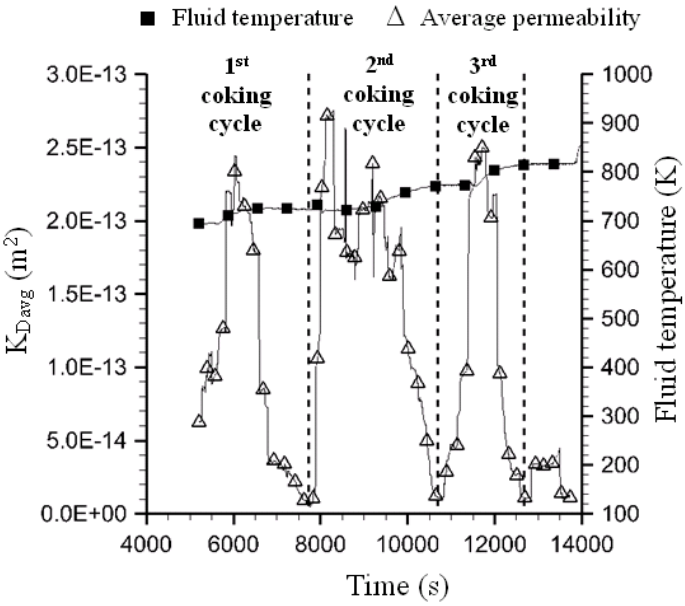

Figure 2. Evolution of the average Darcy permeability and the fluid temperature versus time.

During the initial heating of the system from room temperature to 750K, before the n-dodecane has started to pyrolyse, a constant value of 1.96×10^{-13} m^2 was found for the permeability. This was in full agreement with the value found in the ambient state with a nitrogen flow rate (nonreactive fluid). The vertical lines (dotted) separate the three coking cycles of the porous material. The boundaries between these three cycles (at times 7750 and 10700s) correspond to fluid debits upstream of the porous material at each temperature step. These debits artificially created an inversion in the flow direction for a few instants resulting in the porous material being more or less cleaned. On the contrary, the reductions in Darcy permeabilities were essentially due to the build-up of carbon particles inside the pores of the stainless steel sample. In fact the permeability of the coke deposit (of a thickness of 0.3 mm at the end of the experimentation) on the surface upstream of the material was determined[12] prior to the experiments at approximately 10^{-8} m^2. This high value (with respect to the initial permeability of the medium: 1.96×10^{-13} m^2) should not affect the average Darcy permeability measurement K_{Davg}. This conclusion was reinforced by determining the mass of the carbon deposit detected on the surface (8.66mg) with respect to that inside the sample (460mg) at the end of the experiment. The quantity of coke was 50 times greater in the medium than on the surface. However, on the opposite side of the material there was an absence of carbon deposits. To finish, after each fluid debit (cleaning) a variable time can be observed before there is a reduction in permeability. This is probably due to the chemistry. Because of the differences in temperature, the pyrolysis rate varies considerably (influence of the catalytic effect, presence of certain species previously produced, etc).

Based on the experimental data, it is possible for the thickness of the coked material e_1 to be evaluated using the following relation:

$$e_1 = \frac{V_{coke}}{V_{void}} \times \sum_i e_i \tag{1}$$

where V_{coke}, V_{vide} are respectively the volume of coked material and the volume of the empty spaces whereas e_1 is the thickness of the layer i. The two volumes may be calculated using the following relations:

$$V_{coke} = \frac{m_{coke}}{\rho_{coke}} \tag{2}$$

$$V_{vide} = \frac{\pi}{4} \times d^2 \times \varepsilon \times \sum_i e_i \tag{3}$$

where m_{coke} et ρ_{coke} are respectively the mass and the volumic mass of the coke, d is the diameter of the sample and $\boldsymbol{\varepsilon}$ is the total porosity of the material.
By introducing the two volumes of Eq. (2) and Eq. (3) into Eq. (1), the thickness of the coked material may be expressed by:

$$e_1 = \frac{m_{coke}}{\rho_{coke} \times \frac{\pi}{4} \times d^2 \times \varepsilon} \tag{4}$$

B. Modelling the variability in permeability

In this part, the variability of the permeability within a porous material made of stainless steel will be modelled as it is coking. To perform this work, the database containing the transitional measurements of the average Darcy permeability K_{Davg} described previously is used. On the basis of these transitional measurements of the average permeability, the models developed enable the local permeabilities to be determined as a function of a single space variable $K_D(x)$. The choice of monodimensional models allows the problem to be simplified with regard to the database. Furthermore, models proposed in 1D seem to better reflect reality. Indeed, despite there being strong spatial variability of the permeability in all spatial directions, it seems coherent to assume an even coke face since the fluid tends to continually pass through preferred paths (the fluid drives coke particles which block the former preferred paths). Models of two categories were studied, and namely discontinuous mesh models and continuous analytical models.

1. Discontinuous mesh models

Within the category of discontinuous mesh models, the coking is considered to affect only one part of the thickness (x=3mm) of the porous material. A fist monodimensional model (1D) was developed in which the material is considered to be divided into two meshes of variable lengths e_1 and e_2. The permeabilities K_1 and K_2 are considered to be different and homogeneous in their respective meshes. Then, a second model was developed in which a third mesh of a length e_0 and permeability K_0 was added. The aim was to create a model as close to reality as possible which also integrates the build-up of coke on the surface of the porous material (Fig. 3).

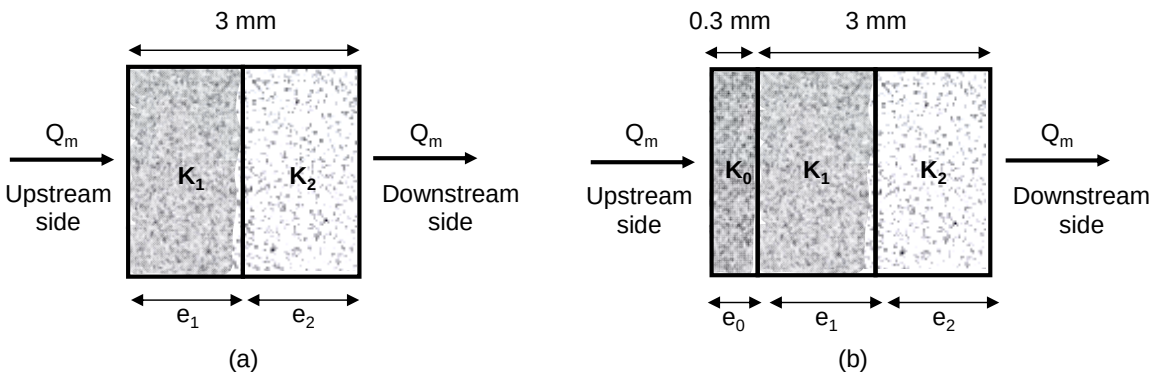

Figure 3. Discretisation model of the porous medium: (a) Model with 2 meshes and (b) Model with 3 meshes.

As mentioned in the introduction, there are different models linking the permeability of each strata (mesh) to the average permeability of the porous material. Although the geometric and arithmetic composition law was tested, the decision was made to retain the harmonic mean (adapted to the problem) to determine the permeability of the mesh influenced by the formation of coke. The relations giving the harmonic mean of the permeability may be expressed as follows[6]:

$$K_{Davg} = \frac{\sum_{j=1}^{n} e_j}{\sum_{j=1}^{n} \frac{e_j}{K_j}} \tag{5}$$

where n is the number of meshes of the porous medium. The principle of the 2 mesh harmonic model is based on the fact that the thickness of the porous material is firstly defined and then the permeability K_2 of the second mesh, which remains constant and has a value of $K_2 = 1.96\text{x}10^{-13}$ m^2 (which is the average permeability of the porous material when not subjected to coking). By using the thickness of the first mesh calculated by the Eq. (1), the permeabilities K_1 in the three coking cycles are deducted from the Eq. (5) by using the value of K_{Davg} at the end of each coking cycle. The permeabilities K_1 are thereafter assumed to be constant and the thickness of the first strata is calculated for the three cycles by using the following relation:

$$e_1(t) = \frac{K_1}{K_{Davg}(t)} e - \frac{K_1}{K_2} e_2 \tag{6}$$

where e = e_1+e_2 is the thickness of the porous sample. With respect to the 3 mesh model, the principle of the harmonic model is based on the addition of a third layer to assimilate the build-up of coke on the surface of the porous medium. In the same way as previously and using the experimental value of K_0 and assuming a linear evolution of the thickness of the layer of coke e_0 versus time, the thickness e_1 may be calculated as a function of time by:

$$e_1(t) = \frac{K_1}{K_{Davg}(t)} e - \frac{K_1}{K_0}(a \times t + b) - \frac{K_1}{K_2} e_2 \tag{7}$$

where parameters a and b may be deduced from the instants at the beginning and end of coking and the final thicknesses of the layer of coke.

2. Continuous analytical models

Within the category of continuous analytical models, the phenomenon of coking is considered to affect the whole of the porous material. The first model chosen is a simple model that stipulates a linear evolution of the Darcy permeability (K_D) as a function of the space variable x (thickness of the porous material) of the form:

$$K_D(x,t) = a(t)x + b(t) \tag{8}$$

where t is the time, $a(t)$ and $b(t)$ are parameters given by the following expression:

$$\begin{cases} a(t) = \frac{2}{e}\left[K_D(t,e) - K_{Davg}(t)\right] \\ b(t) = 2K_{Davg}(t) - K_D(t,e) \end{cases} \tag{9}$$

where $K_D(t,e) = 1.96 \times 10^{-13}\,\text{m}^2$ is the permeability of the material without coking and K_{Davg} the average permeability of the porous material given by the expression:

$$K_{Davg}(t) = \frac{1}{e}\int_0^e K_D(x,t)\,dx \tag{10}$$

In the second continuous analytical model, a spatiotemporal evolution of the local permeability $K_D(x,t)$ is proposed in the form of an exponential equation:

$$K_D(t,x) = \frac{2K_D(t,e)}{1 + \exp\left[\left(1 - \frac{x}{e}\right)\frac{t}{\tau}\right]} \tag{11}$$

where τ is a constant determined by a minimisation of the root-mean square deviation between the theoretical average permeability given by the Eq. (10) and that measured experimentally by using an optimisation algorithm such as a string matching algorithm[15]. The values of this constant as well as the model/experiment comparisons of the average permeabilities are presented in the following section.

III. Results and discussion

In this section, the different models described previously are compared. Firstly, the evolutions in thickness of the first strata versus time, calculated by Eq. (6) and Eq. (7), will be compared. Thereafter, the local permeability values of the two models, linear and exponential, will also be compared. Afterwards, the coking level in the layer with thickness e_1 of the porous material will be evaluated versus time. Lastly, the mass of coke deposits, which is directly linked to this coking level, will be linked to the average Darcy permeability.

A. Temporal evolution in the thickness of the coked material

Figure 4 shows a comparison of the evolution in the coke thickness as a function of time for the three coking cycles. Note that in this study, the final thickness of the coked material is evaluated on the basis of equation (4) and is value is of 1.1 mm. In this Figure, the curves obtained by the 3 mesh harmonic model can be observed to be close to the 2 mesh model. This seems to be linked to the small thickness of the layer of coke e_0 on the surface of the porous material (approximately 0.3mm), which has a high permeability value ($K_0=10^{-8}m^2$) with little impact on the evolution of the thickness of the first layer versus time. The relative errors between these two models are respectively of 2.95%, 3.87% and 4.72% for coking cycles 1, 2 and 3. As can also be observed, the thicknesses of the coke layers e_1 for the three coking cycles increase first gradually and then more quickly. The material can also be observed to become more and more clogged as the coking cycles progress. This observation may be explained by two main factors. The first is the increase in the pyrolysis temperature at each coking cycle, which results in the generation of more reaction products (i.e. coke particles) in the material. The second is the build-up of fine particles which are not all expelled during the cleaning cycles, thereby leading to a quicker blocking of the porous material.

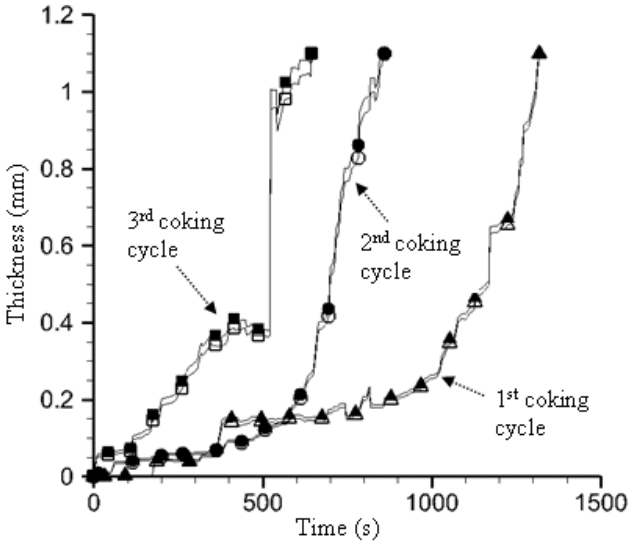

Figure 4. First layer thickness evolution versus time: (filled symbols) model with 2 meshes and (non-filled symbols) model with 3 meshes.

B. Comparison of two models: linear and exponential

As mentioned previously, the exponential model giving the spatio-temporal evolution of the local permeability requires the constant τ to be determined by the minimization of the root-mean square deviation. Figure 5 shows the evolutions versus time of the experimental and theoretical average permeability (calculated on the basis of Eq. (10) and Eq. (11)) of the porous material for the three coking cycles. This Figure shows that the average permeabilities reduced as a function of time. The drop in permeability is rapid at the beginning of coking and then gradually slows down and plateaus at the end of coking. It can be noted that, for a given time, the theoretical permeabilities of cycle 3 are lower than those of cycles 1 and 2. The values of these cycles, however, are close to each other. In other words, the material seems to be clogging up more and more quickly (for the same reasons as those explained previously). It can also be noted that the theoretical curves and the experimental curves of cycle 1 better coincide for values of between 0 and 300 s and between 600 and 1100s. With respect to cycle 2, the theoretical average permeability values are in good agreement with the experimental data for the lapse of time 150-280s, as well as

around 600s. Lastly, the average experimental permeabilities of cycle 3 reinforce the theoretical values of the exponential model for the time lapses 100-450s and 550-650s.

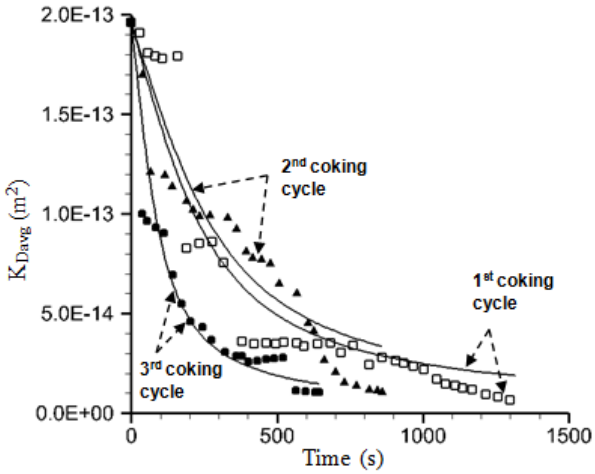

Figure 5. Average permeability evolution as a function of time for 3 coking cycles: symbols represent experimental data and the lines represent the model.

The different values of the constant τ as well as the relative gaps between the theoretical average permeability values and those measured, are shown in Table 1 for the three coking cycles. This Table shows that the parameter τ of coking cycle 3 is greatly inferior to that of cycles 1 and 2. On the contrary, that of cycle 2 is only approximately 1.2 times greater than that of coking cycle 1. Despite the fact that the average theoretical permeabilities are fairly close to the experimental data for most of the time, it does not seem at all obvious to explain the physico-chemical phenomena that are produced by merely using a relatively simple one-parameter model.

	1st Coking cycle	2nd Coking cycle	3rd Coking cycle
τ(s)	91.17	105.97	34.78
Relative gap (%)	4.07	14.17	7.87

Table 1. Values of τ and the relative gap between experimental and theoretical data for different 3 coking cycles.

The two continuous analytical models (linear and exponential) will now be compared. According to Table 1, coking cycle 1 for the exponential model shows the lowest relative error between the experimental and theoretical data for the average permeability. Consequently, it was decided to focus the comparison between the two analytical models on the results of this cycle. Figure 6 shows the spatiotemporal evolution of the permeabilities obtained by the linear and exponential models. This Figure shows that the initial permeabilities as well as those calculated at x=3mm, $\forall t$ are identical for both models. Furthermore, the permeabilities obtained with the linear model are greater than those of the exponential model in the two spatiotemporal regions: $\forall x, t \prec 180s$ and $\forall x \succ 1.5mm,\ t \succ 220s.$ Outside these two regions, it is important to note that the values of the exponential model are greater than those of the linear model. Additionally, the spatiotemporal permeabilities of the exponential model are always positive whereas those of the linear model become negative for $\forall x \prec 1.5mm,\ t \succ 180s.$ Based on these results, it seems clear that the exponential model has greater pertinence in estimating the spatiotemporal evolution of the permeability than the linear model.

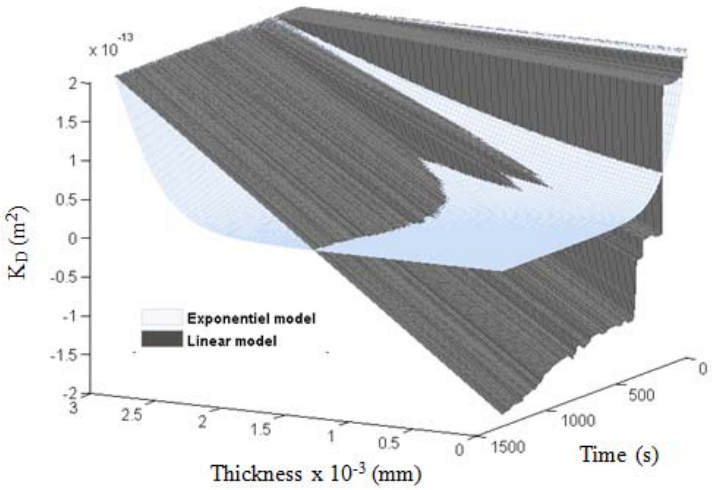

Figure 6. Spatio temporal evolution of permeability obtained by linear and exponential models for 1st coking cycle.

C. Relation between coking and average permeability

This section focuses on the determination of the temporal evolution of the coking rate for the three cycles as well as the average Darcy permeability as a function of the mass of deposited coke.

The coking rate is evaluated using a relation proposed in a previous work[12]:

$$R_{coking}(t) = \frac{\dot{m}_f \times m_{coke}(t)}{\rho_f \times S_g(t) \times V_f(t)} \tag{12}$$

where $\dot{m}_f = 65\,\mathrm{mg \cdot s^{-1}}$ and $\rho_f = 76.21\,\mathrm{kg \cdot m^{-3}}$ are respectively the mass flow rate of the n-dodecane and its volumic mass. The coke mass $m_{coke}(t)$, the total surface area of the steel grains $S_g(t)$ and the volume reserved for the fluid in the coked material $V_f(t)$ are given by the following expressions:

$$m_{coke}(t) = \rho_{coke} \times (\varepsilon - \varepsilon_1) \times \frac{\pi \times d^2}{4} \times e_1(t) \tag{13}$$

$$S_g(t) = \frac{3}{2} \times \pi \times d^2 \times \frac{(1-\varepsilon)}{d_g} \times e_1(t) \tag{14}$$

$$V_f(t) = \varepsilon_1 \times \frac{\pi \times d^2}{4} \times e_1(t) \tag{15}$$

By substituting Eq. (13) to Eq. (15) in Eq. (12), the temporal evolution of the coking rate may be given by:

$$R_{coking}(t) = \frac{2\rho_{coke}}{3\rho_f} \times \frac{\dot{m}_f \times \left(\frac{\varepsilon}{\varepsilon_1} - 1\right) \times d_g}{\pi \times d^2 \times (1-\varepsilon) \times e_1(t)} \tag{16}$$

where ε_1 is the porosity of the coked material, which may be linked to its permeability K_1 and to the steel grain size d_g by the relation[2,16]:

$$\varepsilon_1 = \frac{1}{\frac{d_g}{\sqrt{36 \times h_k \times K_1}} + 1} \tag{17}$$

Figure 7 shows the coking rates in the thickness e_1 of the porous stainless steel, evaluated by Eq. (16) for the three coking cycles. This Figure demonstrates that the initial coking rate of cycle 1 is greater than that of cycle 2, which is itself greater than that of cycle 3. The coking rate of cycle 1 is quasi-constant up to 180 s then decreases very rapidly from this instant to 220s. After this time it slowly varies until reaching the end of the cycle with a quasi-linear trend.

As for the other cycles, the coking rate decreases as the time increases at an exponential rate. It can be observed that for cycle 3, the coking rate reaches an asymptotic value of approximately $4\times10^{-2}\ \mathrm{kg\cdot m^{-2}\cdot s^{-1}}$. A similar tendency was observed[17] for the coking of an aluminium alloy during the decomposition of naphtha at 1098K. The decline in the coking rate as a function of time for the three cycles may be explained by the fact that the contact surface (and thus the catalytic surface) between the material and the n-dodecane reduces as the coke builds up in the thickness e_l of the porous material.

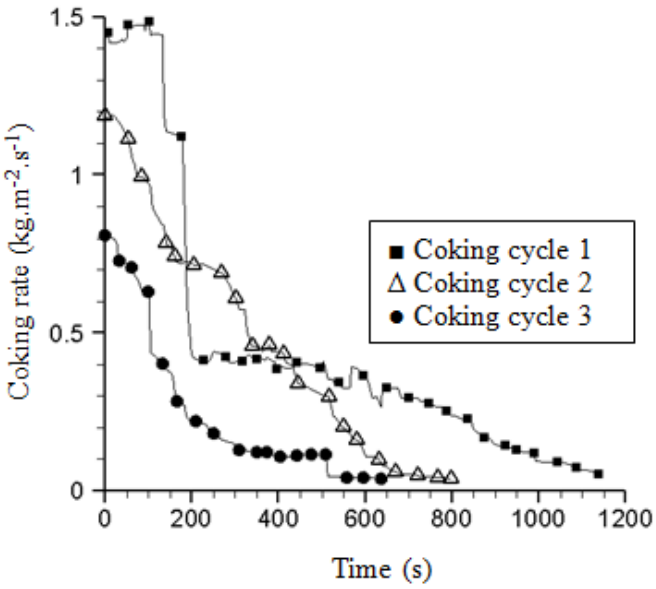

Figure 7. Evolution of the coking rate versus time for the 3 coking cycles.

In practice, the mass of the coke deposit is generally one of the accessible parameters in industrial installations and/or the porous materials within the scope of hydrocarbon cracking. The coking rate is a value that depends on the nature of the fluid, the operating conditions and the type of reactor. The mass of coke deposits is directly linked to this coking rate and it may be usefully linked to the average Darcy permeability. Thus, the transitional models intended to predict the thermal exchange between solid and liquid in the case of structures that are cooled by regeneration will be able to take into account more accurately those changes due to the chemical effect (strongly coupled with multiphase flows with heat and mass transfer). Indeed, Fig. 8 illustrates the evolution (on log-log scales) of the average permeability as a function of the mass of coke deposited in the material for three coking cycles. This Figure shows that the average Darcy permeability decreases quasi-linearly when the mass of coke increases. The values of this permeability for the first coking cycle are lower than for those of the other cycles. Furthermore, the latter two coking cycles have very close permeability values which tends to show the asymptotic behaviour of surface effect on coking compared to homogeneous phase coking rate.

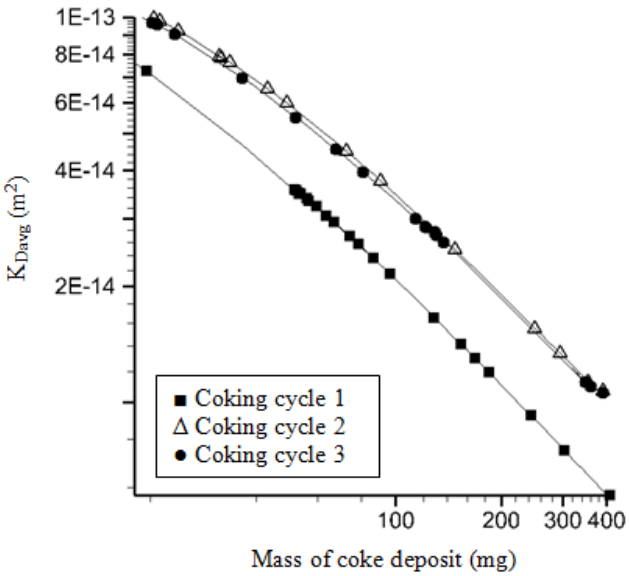

Figure 8. Evolution of the average Darcy permeability versus the mass of coke deposit for the 3 coking cycles.

IV. Conclusion

The purpose of the study was to produce information on the circulation of a reactive fluid (n-dodecane) in a stainless steel porous material, so as to improve understanding of the physical processes involved in active transpiration cooling in aeronautics. Most of this work consisted in developing different models enabling the spatiotemporal variability of the permeability of the stainless steel porous material to be modelled during the coking process. Two categories of models were studies, termed "discontinuous models" and "continuous models". In the discontinuous models, it was assumed that the porous medium was firstly stratified in two and then three layers of different permeabilities. The study revealed that the latter two layers were almost equivalent in evaluating the evolution of the thickness of the coked material versus time. This is no doubt linked to the small thickness of the coke layer at the surface of the porous material and to its high permeability. In the second category, two models (linear and exponential) were proposed and the coke was considered to affect the whole of the thickness of the porous material. Compared to the linear model, the exponential model more adequately describes the spatiotemporal evolution of the permeability. The coking rate in the porous material for the three cycles decreases as a function of time and this decrease may be linked to the reduction in the contact surface between the latter and the fluid. Lastly, the permeability values of the different cycles declines quasi-linearly as a function of the mass of coke deposited inside the porous material.

In future works, the study will be widened to include other materials and fluids. In fact, each material has its own permeability, which depends on the properties, such as the porosity and grain size, of its internal structure. As for the fluid, its capacity to be more or less reactive (to pyrolyse) will also impact the permeability. We are also planning to study the influence of micro-cracking which may appear and increase the permeability of a material over time (given the high pressure and temperature exerted).

References

[1]Gascoin, N., Gillard, P., Bernard, S., and Bouchez, M., "Characterisation of coking activity during supercritical hydrocarbon pyrolysis," *Fuel Process. Technol.*, Vol. 89, 2008, pp. 1416–1428.

[2]Gascoin, N., "High temperature and pressure reactive flows through porous media," *Int. J. Multiphas. Flow*, Vol. 37, 2011, pp. 24–35.

[3]El Tabach, E., Gascoin, N., and Gillard, P., "Neural-Network Metamodelling for the Prediction of the Pressure Drop of a Fluid Passing Through Metallic Porous Medium," *J. Porous Media*, Vol. 17, 2014, pp. 431–438.

[4]Prochazka, P.P., "Time dependent changes of material properties of FRC due to intensive heating," *Mech. Time-Depend. Mater.*, Vol. 18, 2014, pp. 21–39.

[5]El Tabach, E., Lancelot, L., Shahrour, I., and Najjar, Y., "Use of artificial neural network simulation metamodelling to assess groundwater contamination in a road project," *Math. Comput. Model,* Vol. 45, 2007, pp. 766–776.

[6]Tarek, A., *Reservoir Engineering Handbook-Ch. 4: Fundamentals of rock properties, Fourth Edition*, Elsevier, Gulf Professional Publishing, 2010.

[7]dell'Arciprete, D., Bersezio, R., Felletti, F., Giudici, M., Comunian, A., Renard, P., "Comparison of three geostatistical methods for hydrofacies simulation: a test on alluvial sediments," *Hydrogeol. J.*, Vol. 20, No. 2, 2012, pp. 299–311.

[8]De Marsily, G., Delay, F., Gonçalvès, J., Renard, P., Teles, V., and Violette, S., "Dealing with spatial heterogeneity," *Hydrogeol. J.,* Vol. 13, No. 1, 2005, pp. 161–183.

[9]Uh., J., and Watson, A.T., "Determining spatial distributions of permeability," *Transport Porous Med.*, Vol. 86, 2011, pp. 385–414.

[10]Martin III, W.D., Kaye, N.B., and Putman, B.J., "Impact of vertical porosity distribution on the permeability of pervious concrete," *Constr. Build. Mater.*, Vol. 59, 2014, pp. 78–84.

[11]Martin III, W.D., Putman, B.J., and Kaye, N.B., "Using image analysis to measure the porosity distribution of a porous pavement," *Constr. Build. Mater.*, Vol. 48, 2013, pp. 210–217.

[12]Fau, G., Gascoin, N., Gillard, P., Bouchez, M., and Steelant, J., "Fuel pyrolysis through porous media: Coke formation and coupled effect on permeability," *J. Anal. and Appl. Pyrol.*, Vol. 95, 2012, pp. 180–188.

[13]Gascoin, N., Fau, G., Gillard, P., Kuhn, M., Bouchez, M., and Steelant, J., "Comparison of Two Permeation Test Benches and of Two Determination Methods for Darcy's and Forchheimer's Permeabilities," *J. Porous Media*, Vol. 15, 2012, pp. 705–720.

[14]Valdes-Parada, F.J., Ochoa-Tapia, J.A., and Alvarez-Ramirez, J., "On the effective viscosity for the Darcy–Brinkman equation," *Physica A*, Vol. 385, 2007, pp. 69–79.

[15]Chetehouna, K., Séro-Guillaume, O., Sochet, I., and Degiovanni, A., "On the experimental determination of flame front positions and of propagation parameters for a fire," *Int. J. Therm. Sci.,* Vol. 47, 2008, pp. 1148–1157.

[16]Yamamoto, K., Takada, N., and Misawa, M., "Combustion simulation with Lattice Boltzmann method in a three-dimensional porous structure," *P. Combust. Inst.*, Vol. 30, 2005, pp. 1509–1515.

[17]Muñoz Gandarillas, A.E., K.M. Van Geem , Reyniers, M.-F., Marin, G.B., "Influence of the Reactor Material Composition on Coke Formation during Ethane Steam Cracking," *Ind. Eng. Chem. Res*,. Vol. 53, No. 15, 2014, pp. 6358–6371.